nature nanotechnology

LETTERS

PUBLISHED ONLINE: 21 NOVEMBER 2016 | DOI: 10.1038/NNANO.2016.242

# High electron mobility, quantum Hall effect and anomalous optical response in atomically thin InSe

Denis A. Bandurin[1], Anastasia V. Tyurnina[2,3], Geliang L. Yu[1], Artem Mishchenko[1], Viktor Zólyomi[3], Sergey V. Morozov[4,5], Roshan Krishna Kumar[3], Roman V. Gorbachev[3], Zakhar R. Kudrynskyi[6], Sergio Pezzini[7], Zakhar D. Kovalyuk[8], Uli Zeitler[7], Konstantin S. Novoselov[3], Amalia Patanè[6], Laurence Eaves[6], Irina V. Grigorieva[1], Vladimir I. Fal'ko[1,3], Andre K. Geim[1]* and Yang Cao[1,3]*

**A decade of intense research on two-dimensional (2D) atomic crystals has revealed that their properties can differ greatly from those of the parent compound[1,2]. These differences are governed by changes in the band structure due to quantum confinement and are most profound if the underlying lattice symmetry changes[3,4]. Here we report a high-quality 2D electron gas in few-layer InSe encapsulated in hexagonal boron nitride under an inert atmosphere. Carrier mobilities are found to exceed $10^3$ cm$^2$ V$^{-1}$ s$^{-1}$ and $10^4$ cm$^2$ V$^{-1}$ s$^{-1}$ at room and liquid-helium temperatures, respectively, allowing the observation of the fully developed quantum Hall effect. The conduction electrons occupy a single 2D subband and have a small effective mass. Photoluminescence spectroscopy reveals that the bandgap increases by more than 0.5 eV with decreasing the thickness from bulk to bilayer InSe. The band-edge optical response vanishes in monolayer InSe, which is attributed to the monolayer's mirror-plane symmetry. Encapsulated 2D InSe expands the family of graphene-like semiconductors and, in terms of quality, is competitive with atomically thin dichalcogenides[5–7] and black phosphorus[8–11].**

Indium selenide belongs to the family of layered metal chalcogenide semiconductors. Each of its layers has a honeycomb lattice that effectively consists of four covalently bonded Se–In–In–Se atomic planes (see Fig. 1a). The layers are held together by van der Waals interactions at an interlayer distance $d \approx 0.8$ nm. The specific stacking order in bulk γ-InSe, where indium atoms in one layer are aligned with selenium atoms in the other, breaks down the mirror-plane symmetry that is characteristic of monolayer InSe. Earlier studies of bulk InSe revealed a small effective mass in the conduction band[12,13], a high electron mobility at room temperature due to weak electron–phonon scattering[14] and optical activity in absorption and emission[15]. More recently, there have been several reports on thin InSe films made by mechanical exfoliation. Optical studies[16–18] have proved that their bandgaps greatly varied as the number of layers $N$ decreased, in agreement with density functional theory (DFT)[18,19]. Few-layer InSe also exhibits promising characteristics for optoelectronic applications[16,20–22]. Furthermore, the 2D electron gas (2DEG) induced by the field effect at the surface of multilayer (≥20 nm) InSe crystals showed low-temperature mobilities[23,24] $\mu$ of up to 2,000 cm$^2$ V$^{-1}$ s$^{-1}$, approaching the values typically found for the 2D accumulation layers that form near stacking faults in bulk InSe[14,25]. However, the scarcity of experimental data and the spread in the reported characteristics suggest that atomically thin films suffer from considerable degradation with respect to bulk InSe, possibly due to reactions with chemical species present in air, such as oxygen and water (Supplementary Section 6). To circumvent the problem of limited chemical stability, in this work we employ exfoliation and subsequent encapsulation[26,27] of few-layer InSe in an inert (argon) atmosphere[28]. This allowed us to fabricate InSe structures and field-effect devices (FED) down to monolayer thicknesses, and they exhibited previously unattainable qualities and stabilities under ambient conditions.

Figure 1b shows an optical image of a typical InSe flake that has been mechanically exfoliated and visualized inside a glove box filled with argon[28]. The layer thickness was determined from the optical contrast and verified by atomic force microscopy (AFM). To fabricate our FED the exfoliated InSe crystal was transferred onto a hexagonal boron nitride (hBN) flake prepared on a $SiO_2$/doped-Si wafer. Few-layer ($N = 6$–10) graphene (FLG) was positioned on top of the hBN to serve as electrical contacts to the InSe crystal[5], see Fig. 1c. All of the structure was then covered with a second hBN crystal to completely isolate InSe from the environment. Mesas were etched through the top hBN, InSe and FLG to define Hall bars using the gold top gate as the etching mask (Fig. 1d). Finally, Au/Cr contacts to graphene were deposited as shown in Fig. 1c,d and further discussed in Methods. The top hBN flake served as the dielectric layer for the top gate whereas the $SiO_2$/Si wafer acted as the bottom dielectric/gate electrode (Fig. 1c). We studied the electrical properties of six multiterminal InSe devices with thicknesses ranging from 1 to 10 layers.

By applying top and bottom gate voltages ($V_{tg}$ and $V_{bg}$, respectively) we could control the electron density $n$ in InSe over a wide range up to ~$10^{13}$ cm$^{-2}$. We found that the contact resistance between 2D InSe and FLG also depended on gate voltage (Supplementary Section 1). This can be attributed to changes in the Schottky barrier height that depend on doping. Reasonably good ohmic contacts (5–30 kΩ μm) were achieved for $n > 10^{12}$ cm$^{-2}$, allowing four-probe measurements using the standard lock-in technique. In the four-terminal geometry, the sheet resistivity $\rho_{xx}$ of our few-layer InSe devices could be changed between approximately 100 Ω and few kiloohms by varying $V_{bg}$ and $V_{tg}$. Much

[1]School of Physics and Astronomy, University of Manchester, Oxford Road, Manchester M13 9PL, UK. [2]Skolkovo Institute of Science and Technology, Nobel St. 3, 143026 Moscow, Russia. [3]National Graphene Institute, University of Manchester, Manchester M13 9PL, UK. [4]Institute of Microelectronics Technology and High Purity Materials, RAS, Chernogolovka 142432, Russia. [5]National University of Science and Technology 'MISiS', Leninsky Pr. 4, 119049 Moscow, Russia. [6]School of Physics and Astronomy, University of Nottingham, Nottingham NG7 2RD, UK. [7]High Field Magnet Laboratory (HFML –EMFL), Radboud University, Toernooiveld 7, 6525 ED Nijmegen, The Netherlands. [8]National Academy of Sciences of Ukraine, Institute for Problems of Materials Science, UA-58001 Chernovtsy, Ukraine. *e-mail: geim@manchester.ac.uk; yang.cao@manchester.ac.uk

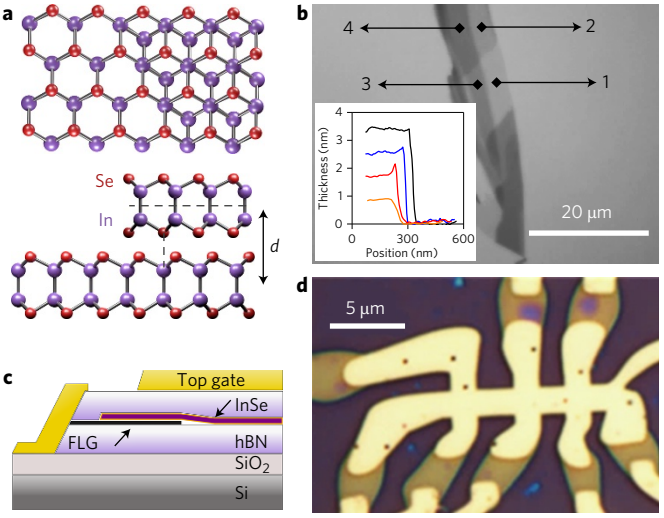


**Figure 1 | 2D InSe devices. a**, Schematic of the mono- and bilayer crystal structures. Purple and red spheres correspond to indium and selenium atoms, respectively. **b**, Micrograph of an InSe flake exfoliated onto a 300-nm-thick polymer film. Numbers 1–4 correspond to *N*, as determined by AFM. Inset: AFM profiles with respect to the polymer substrate. **c**, Cross-sectional schematic of our FEDs. **d**, Optical micrograph of a device. The central bright area is the top gate that covers the encapsulated InSe. Peripheral Au contacts lead to hBN-encapsulated FLG that is not covered by the top gate; the FLG region is dark yellow.

higher resistivities were achieved by applying negative gate voltages (removing electrons from the channel) but this allowed only two-probe measurements because of very high channel and contact resistances (Supplementary Section 3).

Examples of the dependence of $\rho_{xx}$ on $V_{bg}$ are shown in Fig. 2a for a six-layer (6L) device. The resistivity increases with temperature $T$ for all gate voltages, indicating metallic behaviour. Carrier density $n$ was determined from Hall measurements, and its values for different $V_{bg}$ agree with the concentrations estimated from the device geometrical capacitance (inset of Fig. 2a). Figure 2b shows the values of Hall mobility, $\mu = 1/ne\rho_{xx}$, as a function of $T$ for various $n$ accessible in our four-probe measurements, where $e$ is the electron charge. Below 50 K, $\mu$ is almost independent of $T$ and is instead limited by disorder. Its screening by a high density of electrons leads to an increase in $\mu$, and our best device exhibited an electron mobility of 12,700 $cm^2\,V^{-1}\,s^{-1}$ for $n \approx 8 \times 10^{12}$ $cm^{-2}$. For $T > 100$ K, we observed a gradual decrease in $\mu$, faster than the standard $T^{-1}$ dependence expected for acoustic phonon scattering in the Bloch–Gruneisen regime[29]. This can be attributed to additional scattering at homopolar optical phonons with a low activation energy of ~13 meV (see ref. 19). At room temperature, $\mu$ drops to ~1,000 $cm^2\,V^{-1}\,s^{-1}$, which is higher than the highest mobility reported for 2D dichalcogenides[5,7] and comparable to that of black phosphorus[11]. Similar behaviour was found for 3L and 10L devices (inset of Fig. 2b and Supplementary Section 4).

Figure 3 shows the behaviour of $\rho_{xx}$ and Hall resistivity $\rho_{xy}$ in magnetic field $B$ for our 3L and 6L devices (data for a 10L device are provided in Supplementary Section 4). In the 6L device, Shubnikov de Haas oscillations (SdHO) start at $B \approx 4.5$ T, which yields a quantum mobility of about 2,200 $cm^2\,V^{-1}\,s^{-1}$, close to the Hall mobility measured for the same $n$ (Fig. 2b). In high $B$, SdHO developed into the quantum Hall effect so that $\rho_{xx}$ diminished and $\rho_{xy}$ exhibited plateaux (Fig. 3a,f). Figure 3b,c provides further details about how the amplitude and phase of the SdHO evolve with $B$ and $n$. In particular, the Landau fan diagram in Fig. 3c plots the $B$ values in which minima of the oscillations occur. Each set of the minima can be extrapolated to zero (with an experimental uncertainty of ±15%), proving that SdHO in 2D InSe have the standard phase. This means that, unlike graphene, 2D InSe exhibits no Berry phase[3], in agreement with general expectations. Furthermore, the period of the SdHO, $\Delta(1/B)$, allowed independent measurement of the electron density as $n = (2e/h)(1/\Delta(1/B))$ where $h$ is Planck's constant and the pre-factor 2 accounts for spin degeneracy. The obtained values agree well with the densities measured in the same device using the Hall effect (inset of Fig. 3c). This indicates that all conduction electrons reside within a single electric subband and within a single valley, in agreement with the band structure calculations in Supplementary Section 7. This is in contrast to the behaviour observed for 2DEGs that formed at stacking faults in bulk InSe where, despite smaller carrier densities, four

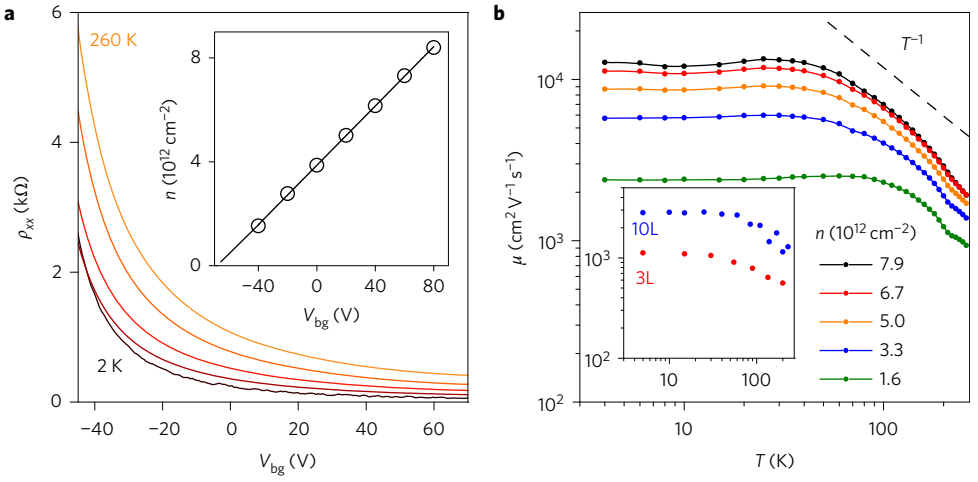


**Figure 2 | Transport properties of atomically thin InSe. a**, The resistivity of a 6L device as a function of $V_{bg}$ at different $T$. Additional top gate voltage ($V_{tg}$ = 8 V) was applied to increase $n$ in the 2DEG. For negative gate voltages ($V_{bg} < -45$ V), the contact resistance increased above 100 kΩ, which did not permit four-probe measurements. Large on/off ratios, similar to those in previous reports[23,24], could be measured in the two-probe geometry (Supplementary Section 3). Inset: $n$ found from Hall measurements (symbols); the solid line shows the density expected from the known geometrical capacitance. **b**, $T$ dependence of the Hall mobility $\mu$ for the 6 L device. The dashed black line shows the dependence expected for acoustic phonons. Inset: $\mu$ ($T$) for 3 and 10 L at high doping (8.3 and 7.7 × $10^{12}$ $cm^{-2}$, respectively).

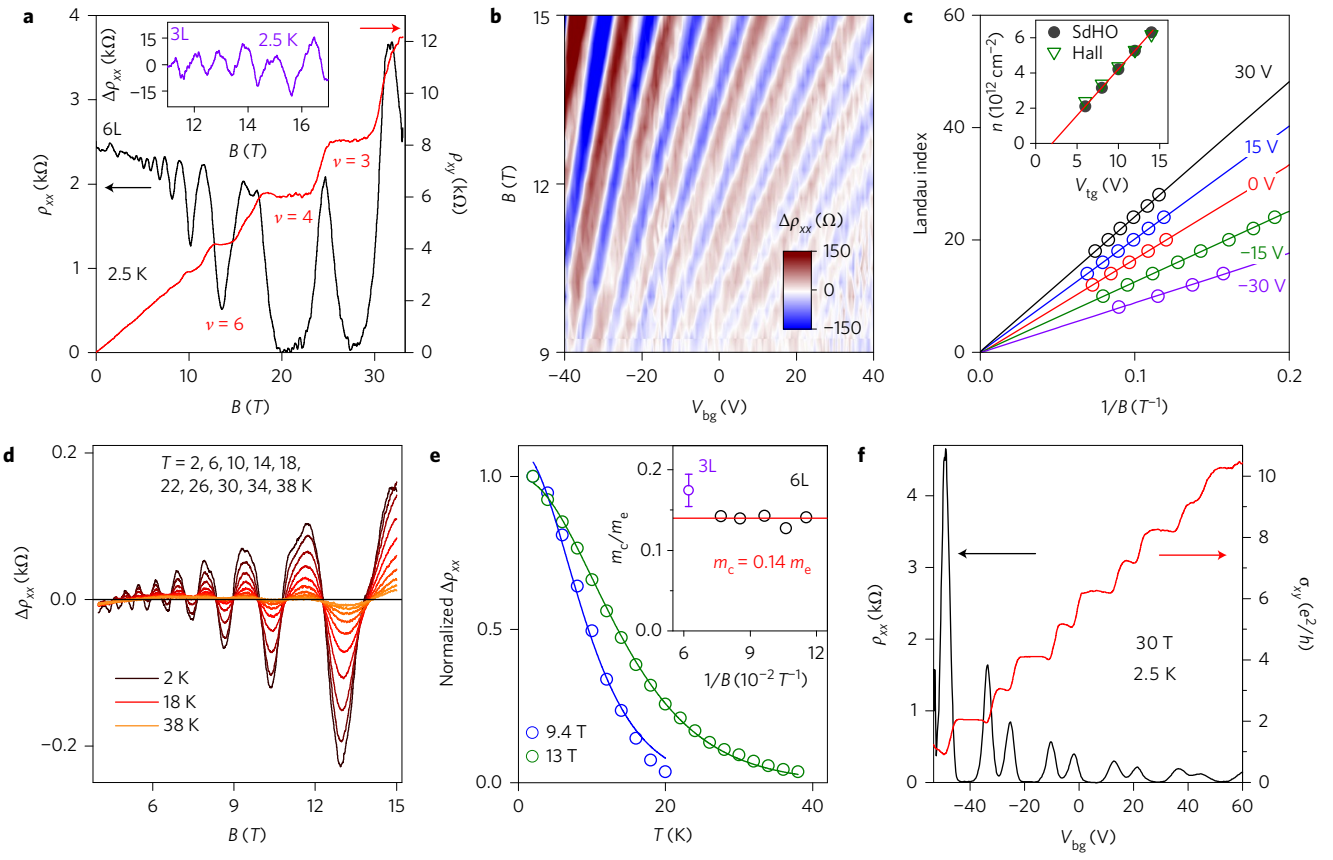


**Figure 3 | Magnetotransport in few-layer InSe. a**, Low-$T$ $\rho_{xx}$ and $\rho_{xy}$ for our 6L device; $n = 2 \times 10^{12}$ cm$^{-2}$. Inset: SdHO in 3L InSe; $n = 8.9 \times 10^{12}$ cm$^{-2}$ and the smooth non-oscillating background is subtracted. **b**, Colour map of SdHO amplitude, $\Delta\rho_{xx}(V_{bg}, B)$, in the 6L FED at $V_{tg} = 8$ V and 5 K. **c**, Minima in the SdHO shown in **b** as a function of $1/B$ for several $V_{bg}$ values. Inset: Carrier densities as a function of $V_{tg}$ determined from Hall measurements and SdHO. The red line is $n$ expected from the geometrical capacitance; $V_{bg} = -10$ V. **d**, Temperature dependence of $\Delta\rho_{xx}$ for 6L InSe; $n = 2.5 \times 10^{12}$ cm$^{-2}$. **e**, Examples of $\Delta\rho_{xx}(T)$ shown in **d** at fixed $B$ and normalized by the corresponding values at 2 K. Solid lines are best fits from the Lifshitz–Kosevich formula, which also yield the Dingle temperature of ~10 K. Inset: Cyclotron masses found for $N = 3$ and 6. Error bars for the 6L data are given by the size of the circles. The red line shows $m_e$ in bulk InSe. **f**, Quantum Hall effect in the 6L device as a function of $V_{bg}$ using $V_{tg} = 8$ V.

sets of SdHO were found originating from different electric subbands[25]. We observed some population of the second subband only in 10L InSe (Supplementary Section 4). The difference with bulk InSe is attributed to much stronger quantum confinement in our atomically thin crystals, which significantly increases the energy separation between subbands.

The SdHO were pronounced over a wide range of $T$ (Fig. 3d), which enabled us to determine the effective mass, $m_c$, of electrons in few-layer InSe. For 6L, the best fit of the SdHO amplitude using the Lifshitz–Kosevich formula yielded $m_c = 0.14 \pm 0.01\ m_e$, which is close to the bulk value[13] (Fig. 3e). A heavier $m_c \approx 0.17 \pm 0.02\ m_e$ was found for 3L InSe, where $m_e$ is the free electron mass. The high quality of the 2DEG in our 6L device allowed the observation of the fully developed quantum Hall effect. Figure 3f shows behaviour of $\rho_{xx}$ and Hall conductivity $\sigma_{xy}$ with changing electric doping at $B = 30$ T. While $\sigma_{xy}$ exhibits plateaux close to the quantized values $\nu e^2/h$ (where $\nu$ is an integer), the resistivity drops to zero for the corresponding intervals of $V_{bg}$. We observed quantum Hall plateaux for all odd and even $1 \leq \nu \leq 10$, indicating a lifted spin degeneracy. The temperature dependence of the minimum in $\rho_{xx}$ at $\nu = 3$ was carefully measured, which allowed a rough estimate of the effective $g$ factor of $g \approx 2$ (Supplementary Section 5).

Despite several attempts, we were unable to achieve sufficiently high conductance in the 1L devices to carry out successful four-probe measurements (Supplementary Section 2). Even at the highest doping, our monolayer FEDs exhibited two-probe resistances larger than 1 MΩ. The field-effect mobility extracted in the two-terminal geometry was <0.1 cm$^2$ V$^{-1}$ s$^{-1}$ but note that, unlike the Hall mobility, this measure is likely to be dominated by changes in the contact resistance[24]. Except for graphene, all other monolayer crystals studied so far[2,28,30] exhibited similarly low electronic quality. This can be related to stronger degradation of the ultimately thin films[31]. However, other scenarios are also possible. For example, the large bandgap in monolayer InSe (predicted theoretically and reported below) should favour a larger density of midgap states, making it difficult to fill them and reach the conduction band edge. In addition, larger gaps usually result in higher Schottky barriers and, therefore, a higher contact resistance can be expected for the graphene–InSe interface.

To gain further information about few-layer InSe, we employed photoluminescence (PL) spectroscopy. Figure 4 shows the PL response found for hBN-encapsulated InSe crystals using laser excitation at photon energies of 2.3, 2.7 and 3.8 eV (see Methods). We studied 2D crystals with every value of $N$ from 1 to 8. For 2–8 layer InSe, their PL spectra showed two lines, $A$ at a lower and $B$ at a higher energy, whereas monolayer InSe exhibited only the high-energy peak. The inset of Fig. 4a plots the energy of the $A$ and $B$ lines for different $N$, with dots corresponding to the measured PL and open squares to the DFT calculations described in Supplementary Section 7. The progressive blueshift of the $A$ line with decreasing $N$ follows the trend reported previously[17,18]. To highlight the disappearance of the $A$ line in 1L InSe, Fig. 4b

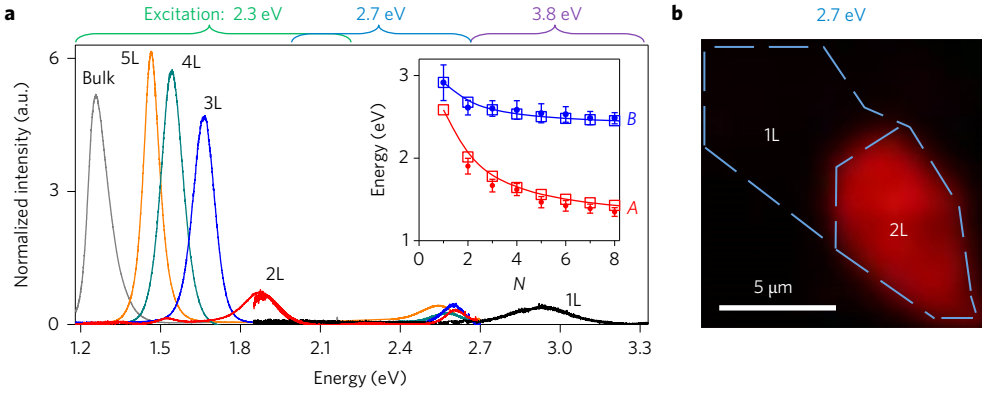


**Figure 4 | Photoluminescence from 2D InSe. a**, PL spectra measured at room temperature using three excitation energies. The corresponding ranges of the PL detection are indicated above. Excitation at 2.3 eV generated the *A* peak in *N*-layer crystals and bulk InSe (~45 nm). Excitation by 2.7 and 3.8 eV lasers resulted in the *B* peak for all *N*. The intensities are normalized by the number of layers, except for bulk InSe for which the intensity is normalized to fit the scale. Note that the spectral peak at 1.9 eV for 2L InSe was accessible in both 2.3 and 2.7 eV excitation measurements, and the two red curves overlap. Inset: Energies of the *A* and *B* peaks for different *N*, with the error bars indicating the PL linewidth. The squares, connected by solid curves, show our DFT results. **b**, Map of PL intensity integrated over the spectral range 1.85–2.7 eV for excitation at 2.7 eV. The blue contours indicate the position of mono- and bilayer regions. The black to red colour scale indicates the intensity variations from zero to maximum.

shows a PL intensity map for a device containing mono- and bilayer regions. There was no discernable PL response in the *A* spectral region anywhere within the 1L area.

To explain the observed PL behaviour, we have carried out DFT calculations of the band structure of 2D InSe using its monolayer as a building block for thicker films. The results are summarized in the inset of Fig. 4a and detailed in Supplementary Section 7. The observed decrease in the PL energies with increasing *N* can be explained as follows. The electronic bands of 1L InSe split into *N* subbands in the *N*-layer crystal, and this reduces the energy difference between the conduction and valence states in the vicinity of the Γ point at which the bandgap is smallest[18,19]. This leads to a decrease in the principal (optical) bandgap that gives rise to the *A* peak. A smaller reduction occurs for the *B* peak that involves deeper, less-affected valence bands (Supplementary Fig. 7). Furthermore, because of the mirror-plane symmetry ($z \rightarrow -z$) for 1L InSe, wavefunctions for electronic states near the edges of the valence and conduction bands are even and odd with respect to transformation $z \rightarrow -z$, respectively[19,23]. This makes the lowest-energy electron–hole transition (at ~2.6 eV as found by DFT; inset of Fig. 4a) optically inactive for in-plane polarized light[18,19] and only weakly coupled to *z*-polarized light. In few-layer InSe, the mirror symmetry is broken (see Fig. 1a), which promotes coupling to in-plane polarized light and gives rise to the optical transitions responsible for the *A* line. Coupling to *z*-polarized light also increases with *N* (see Supplementary Section 7). In contrast, two deeper valence bands at the Γ point in 1L InSe have odd wavefunctions giving rise to the *B* peak at ~2.9 eV. The symmetry for this transition is largely unaffected by increasing *N*. The relatively high visibility of the *B* line in 2D InSe comes from the fact that, according to our DFT calculations, wavefunctions of electronic states in different valence bands differ so substantially that electron–phonon relaxation between them and Auger recombination are greatly suppressed.

To conclude, hBN-encapsulation of atomically thin InSe in an oxygen- and moisture-free atmosphere allows high-quality optics and electron transport devices, which is difficult to achieve otherwise. Because InSe exhibits a higher environmental stability than few-layer black phosphorous and a higher room-temperature mobility and lighter electron mass than few-layer dichalcogenides, our work indicates a promising playground for studying low-dimensional phenomena and an interesting venue for developing ultrathin-body high-mobility nanoelectronics. In terms of optics, monolayer InSe features strongly suppressed recombination of electron–hole pairs, which can be used to pump the system to high exciton densities that are potentially suitable for studying excitonic complexes and exciton condensation.

## Methods

Methods and any associated references are available in the online version of the paper.

Received 26 June 2016; accepted 10 October 2016;
published online 21 November 2016

## References

1. Novoselov, K. S. *et al.* Two-dimensional atomic crystals. *Proc. Natl Acad. Sci. USA* **102,** 10451–10453 (2005).
2. Geim, A. K. & Grigorieva, I. V. Van der Waals heterostructures. *Nature* **499,** 419–425 (2013).
3. Castro Neto, A. H., Peres, N. M. R., Novoselov, K. S. & Geim, A. K. The electronic properties of graphene. *Rev. Mod. Phys.* **81,** 109–162 (2009).
4. Mak, K. F., Lee, C., Hone, J., Shan, J. & Heinz, T. F. Atomically thin $MoS_2$: a new direct-gap semiconductor. *Phys. Rev. Lett.* **105,** 2–5 (2010).
5. Cui, X. *et al.* Multi-terminal transport measurements of $MoS_2$ using a van der Waals heterostructure device platform. *Nat. Nanotech.* **10,** 534–540 (2015).
6. Fallahazad, B. *et al.* Shubnikov–de Haas oscillations of high-mobility holes in monolayer and bilayer $WSe_2$: Landau level degeneracy, effective mass, and negative compressibility. *Phys. Rev. Lett.* **116,** 086601 (2016).
7. Xu, S. *et al.* Universal low-temperature ohmic contacts for quantum transport in transition metal dichalcogenides. *2D Mater.* **3,** 021007 (2016).
8. Tayari, V. *et al.* Two-dimensional magnetotransport in a black phosphorus naked quantum well. *Nat. Commun.* **6,** 7702 (2015).
9. Li, L. *et al.* Quantum oscillations in a two-dimensional electron gas in black phosphorus thin films. *Nat. Nanotech.* **10,** 608–613 (2015).
10. Gillgren, N. *et al.* Gate tunable quantum oscillations in air-stable and high mobility few-layer phosphorene heterostructures. *2D Mater.* **2,** 011001 (2014).
11. Li, L. *et al.* Quantum Hall effect in black phosphorus two-dimensional electron system. *Nat. Nanotech.* **11,** 6–10 (2016).
12. Kuroda, N. & Nishina, Y. Resonance Raman scattering study on exciton and polaron anisotropies in InSe. *Solid State Commun.* **34,** 481–484 (1980).
13. Kress-Rogers, E., Nicholas, R. J., Portal, J. C. & Chevy, A. Cyclotron resonance studies on bulk and two-dimensional conduction electrons in InSe. *Solid State Commun.* **44,** 379–383 (1982).
14. Segura, A., Pomer, F., Cantarero, A., Krause, W. & Chevy, A. Electron scattering mechanisms in *n*-type indium selenide. *Phys. Rev. B* **29,** 5708–5717 (1984).
15. Camassel, J., Merle, P., Mathieu, H. & Chevy, A. Excitonic absorption edge of indium selenide. *Phys. Rev. B* **17,** 4718–4725 (1978).
16. Lei, S. *et al.* Evolution of the electronic band structure and efficient photo-detection in atomic layers of InSe. *ACS Nano* **8,** 1263–1272 (2014).
17. Mudd, G. W. *et al.* Tuning the bandgap of exfoliated InSe nanosheets by quantum confinement. *Adv. Mater.* **25,** 5714–5718 (2013).

18. Brotons-Gisbert, M. *et al.* Nanotexturing to enhance photoluminescent response of atomically thin indium selenide with highly tunable band gap. *Nano Lett.* **16,** 3221–3229 (2016).
19. Zolyomi, V., Drummond, N. D. & Fal'ko, V. I. Electrons and phonons in single layers of hexagonal indium chalcogenides from *ab initio* calculations. *Phys. Rev. B* **89,** 1–8 (2014).
20. Feng, W. *et al.* Ultrahigh photo-responsivity and detectivity in multilayer InSe nanosheets phototransistors with broadband response. *J. Mater. Chem. C* **3,** 7022–7028 (2015).
21. Mudd, G. W. *et al.* High broad-band photoresponsivity of mechanically formed InSe–graphene van der Waals heterostructures. *Adv. Mater.* **27,** 3760–3766 (2015).
22. Tamalampudi, S. R. *et al.* High performance and bendable few-layered InSe photodetectors with broad spectral response. *Nano Lett.* **14,** 2800–2806 (2014).
23. Feng, W., Zheng, W., Cao, W. & Hu, P. Back gated multilayer InSe transistors with enhanced carrier mobilities via the suppression of carrier scattering from a dielectric interface. *Adv. Mater.* **26,** 6587–6593 (2014).
24. Sucharitakul, S. *et al.* Intrinsic electron mobility exceeding $10^3$ $cm^2/Vs$ in multilayer InSe FETs. *Nano Lett.* **15,** 3815–3819 (2015).
25. Kress-Rogers, E. *et al.* The electric sub-band structure of electron accumulation layers in InSe from Shubnikov–de Haas oscillations and inter-sub-band resonance. *J. Phys. C* **16,** 4285–4295 (2000).
26. Wang, L. *et al.* One-dimensional electrical contact to a two-dimensional material. *Science* **342,** 614–617 (2013).
27. Kretinin, A. V. *et al.* Electronic properties of graphene encapsulated with different two-dimensional atomic crystals. *Nano Lett.* **14,** 3270–3276 (2014).
28. Cao, Y. *et al.* Quality heterostructures from two-dimensional crystals unstable in air by their assembly in inert atmosphere. *Nano Lett.* **15,** 4914–4921 (2015).
29. Sun, C. *et al. Ab initio* study of carrier mobility of few-layer InSe. *Appl. Phys. Express* **9,** 035203 (2016).
30. Castellanos-Gomez, A. Why all the fuss about 2D semiconductors? *Nat. Photon.* **10,** 202–204 (2016).
31. Favron, A. *et al.* Photooxidation and quantum confinement effects in exfoliated black phosphorus. *Nat. Mater.* **14,** 826–832 (2015).


## Acknowledgements

This work was supported by the European Research Council, the Graphene Flagship, the Engineering and Physical Sciences Research Council (EPSRC, UK) and The Royal Society. D.A.B. and I.V.G. acknowledge support from the Marie Curie programme SPINOGRAPH (Spintronics in Graphene). A.M. acknowledges support of the EPSRC Early Career Fellowship EP/N007131/1. S.V.M. was supported by the NUST MISiS (grant K1-2015-046) and the Russian Foundation for Basic Research (RFBR15-02-01221 and RFBR14-02-00792). V.F. acknowledges support from the ERC Synergy Grant Hetero2D, the EPSRC grant EP/N010345/1 and the Lloyd Register Foundation Nanotechnology grant, and V.Z. from the European Graphene Flagship Project. Measurements in high magnetic field were supported by the High Field Magnet Laboratory–Radboud University/Foundation for Fundamental Research on Matter, member of the European Magnetic Field Laboratory, and by the EPSRC via its membership to the EMFL (grant EP/N01085X/1). We thank M. Mohammed for assisting with UV PL measurements.

## Author contributions

D.A.B., G.L.Y., R.K.K., A.M. and S.V.M. performed transport measurements and A.V.T. carried out optical studies. D.A.B. and A.V.T. analysed experimental data with help from A.K.G. and V.I.F. Y.C. fabricated devices and co-supervised the project with help from R.V.G. V.Z. and V.I.F. provided theory support. Z.R.K., Z.D.K. and A.P. provided bulk InSe crystals. D.A.B., V.I.F. and A.K.G. wrote the manuscript. All authors contributed to discussions.

## Additional information

Supplementary information is available in the online version of the paper. Reprints and permissions information is available online at www.nature.com/reprints. Correspondence and requests for materials should be addressed to A.K.G. and Y.C.

## Competing financial interests

The authors declare no competing financial interests.

## Methods

**Sample preparation.** InSe devices were prepared using mechanical exfoliation and hBN encapsulation, which were carried out in an inert atmosphere in a glovebox. Thin InSe crystallites were first exfoliated from Bridgman-grown bulk γ-InSe onto a 300 nm layer of polymethyl glutarimide (PMGI). Their thickness was identified in an optical microscope and selectively verified by AFM. Then we used the dry peel transfer technique[26,27] to pick up a chosen InSe crystal with a larger hBN flake attached to a polymer membrane. The resulting hBN–InSe stack was transferred onto a relatively thick (>50 nm) hBN crystal prepared on top of an oxidized Si wafer. The latter hBN flake had two narrow ribbons of FLG prepared on top of it. During the final transfer, the crystals were aligned so that edges of the InSe overlapped with the FLG to provide an ohmic contact[5]. Such encapsulation not only protected ultrathin InSe during the following fabrication but also protected its surfaces from contamination[28].

The assembled hBN/Gr/InSe/hBN heterostructure was removed from the glovebox Ar environment and patterned using electron beam lithography to create quasi-one dimensional contacts to the FLG[27]. As metallic contacts, we deposited 3 nm of Cr followed by 50 nm Au. The next round of e-beam lithography was used to define a top gate that was in a shape of a multiterminal Hall bar. The metal top gate then served as an etch mask for reactive ion etching, which translated the Hall bar shape into InSe. The final devices were fully protected from the environment, except for the exposed etched edges[26,27], and did not show any signs of deterioration over many months.

**PL measurements.** Several encapsulated InSe structures were prepared to analyse their PL response. Typically, they were multi-terraced flakes that contained parts of different thickness from bulk InSe down to a monolayer. PL measurements were performed at room temperature using three different optical set-ups to cover the widest possible spectral range. To study PL between 1.2 and 2.3 eV we used HORIBA's Raman system XploRA PLUS with a laser of wavelength 532 nm (spot size ~1 μm, laser power of 1.35 mW and the spectrometer grating of 600 groves per millimetre). For the midrange energies from 1.8 to 2.7 eV we used Renishaw system InVia equipped with a 457 nm laser (spot size ~1 μm, laser power of 0.2 mW and 2,400 groves per millimetre). To detect PL from monolayer InSe, it was necessary to extend the spectral range and we used Horiba LabRAM HR Evolution (UV laser at 325 nm with the beam spot size of ~2 μm, laser power of 1.2 mW and grating of 600 groves per millimetre). This allowed us to detect PL in the range from 2.7 to 3.8 eV. For each set-up, spectra were collected using the same acquisition parameters (time and focus distance), and an additional spectrum from an area near the tested sample (without InSe) was acquired as a reference. The reference signal was subtracted from the spectra from *N*-layer regions. The resulting curves were normalized per absorbing layer, as mentioned in the caption of Fig. 4. For 1L InSe, accurate normalization was not possible because of the absence of the lower-energy *A* peak in PL. However, one can see that the intensity of the *B* peak in Fig. 4a does not vary significantly with *N* for other thicknesses, which makes the reported intensity for 1L correct, at least qualitatively.